ELSEVIER

Materials Science and Engineering A 421 (2006) 328–337

MATERIALS SCIENCE & ENGINEERING A

www.elsevier.com/locate/msea

Phase equilibria and solidification of Mg-rich Mg–Al–Zn alloys

M. Ohno, D. Mirkovic, R. Schmid-Fetzer *

Institute of Metallurgy, Clausthal University of Technology, Robert-Koch-Str. 42, D-38678 Clausthal-Zellerfeld, Germany

Received 1 September 2005; accepted 1 February 2006

Abstract

Phase equilibria in Mg-rich corner of Mg–Al–Zn system are analyzed in detail. Thermodynamic calculations are compared with literature data and own key experimental results by means of DSC and DTA measurements. The detailed comparison strongly supports the reliability of the selected thermodynamic description. Furthermore, our focus is placed on proper interpretation of experimental results obtained by thermal analysis. Based on thermodynamic calculation, it is clarified that a signal observed in thermal analysis, which was interpreted as end of solidification in the literature, is related to the start of the monovariant eutectic reaction L + (Mg) + γ-$Mg_{17}Al_{12}$ under non-equilibrium condition and the solidification process ends at lower temperature. This fact is supported by our microstructural observation.

Keywords: Magnesium-alloy; Calphad; Phase diagram; Scheil solidification; Differential scanning calorimetry

1. Introduction

Phase equilibria of the Mg–Al–Mn–Zn quaternary system provide crucial information in development and designing of Mg-alloys like the significant AZ and AM series. The main goal of the series of present studies is to establish the thermodynamic description for the Mg–Al–Mn–Zn system on the basis of well assessed and properly interpreted experimental data. To this end, the thermodynamic description for each sub-ternary system as well as sub-binary system needs to be obtained, scrutinized or improved to compute the phase equilibria with high precision. The thermodynamic description for the Mg-rich corner of the Al–Mg–Mn system has been recently improved by the present authors [1]. In this paper, we focus on the Mg–Al–Zn ternary system.

The thermodynamic description of Mg–Al–Zn system has been reported by Liang et al. [2]. They performed the experimental investigation on the ternary solubilities of the Al–Mg and Mg–Zn phases as well as the homogeneity ranges of ternary compounds τ and ϕ phases by means of X-ray diffraction (XRD), differential thermal analysis (DTA), differential scanning calorimetry (DSC) and electron probe microanalysis (EPMA). Then, the thermodynamic description was obtained based on their experimental data and available literature data. They showed the comparison between the calculated and experimental results concerning invariant reaction temperatures, isothermal section at 608 K and some vertical sections, and the satisfying agreement was presented.

Since the focus of Liang et al. [2] was placed on the entire composition range, the detailed comparison regarding Mg-rich corner was not demonstrated and the reliability of their thermodynamic description for Mg-rich corner has not been fully discussed. For the practical application of Calphad approach to development of Mg-alloys, the accuracy and precision of the calculated phase equilibria are significant to know. In the present paper, we firstly demonstrate the detailed comparison between results calculated using the thermodynamic description of Liang et al. [2] and the experimental data, with a view to proving the reliability of the calculated phase equilibria. Our focus is on the composition range of Mg-rich corner, 0–30 wt.% Al and 0–30 wt.% Zn. One will see that the calculated results are quite consistent with the experimental data.

In the present study, subsequently, a particular attention is directed to the composition range, 0–10 wt.% Al and 0–3 wt.% Zn, which is quite important range from the point of view of industrial applicability of Mg-alloys. Since highly precise analysis on the phase equilibria in this composition range has not been carefully performed by means of current sophisticated equipment, we carried out own key experiments of DSC and DTA measurements with Ta crucible. A proper interpretation of the

* Corresponding author. Tel.: +49 5323 72 2150; fax: +49 5323 72 3120.
E-mail address: schmid-fetzer@tu-clausthal.de (R. Schmid-Fetzer).

0921-5093/$ – see front matter © 2006 Elsevier B.V. All rights reserved.
doi:10.1016/j.msea.2006.02.006

experimental result is in the focus of this discussion. From our measurement, it is demonstrated that the equilibrium solidification process can hardly be realized in Mg-rich alloys even with the cooling rate of 1 K/min. More importantly, one will see that the thermal signal observed at low temperature, which has been interpreted as end of solidification in the literature, is not the true solidus temperature and solidification process finishes at lower temperature.

2. Experimental data in literature

The experimental results for the entire Mg–Al–Zn system have been assessed by Petrov [3]. Also, the phase diagrams drawn in the experimental works have been compiled by Villars et al. [4]. As mentioned in Section 1, we focus on the composition range 0–30 wt.% Al and 0–30 wt.% Zn. In the following, the experimental works relevant to this composition range are briefly summarized.

Liquidus surface for Mg-rich corner has been investigated by means of thermal analysis in several works [5–10]. In the papers [9,10], however, the actual values of the measured liquidus temperature were not clearly shown and only the constructed phase diagrams were demonstrated. In the present study, their results are not employed for the comparison. The primary precipitates were identified on the basis of microstructural observation [5–8], however, the alloy compositions employed for the determination of the primary precipitate were clearly indicated only in Refs. [7,8]. While an extremely wide primary phase field of $MgZn_2$ was shown in Ref. [7], a part of the wide $MgZn_2$ field was replaced by primary phase field of ternary τ-phase in the later assessment [3].

The thermal analysis down to low temperature region for Mg-rich corner has been performed in several works [5–8]. Furthermore, in the work of Hamasumi [7], the number of equilibrium phases at various composition and temperatures was determined based on the microstructural observation of quenched samples.

The solidus isotherms have been presented by Mikheeva and Krjukova [11]. Furthermore, the solvus curves for the Mg-solid solution were determined from the microstructural observation. In their work [11], however, the detail of the experimental method was not explained and the actual values of the experimental data were not given. The solvus isotherms of Mg-solid solution were also demonstrated by Busk and Marande [10], however, again the actual values of experimental data were not given.

Clark investigated the phase equilibria for Mg-rich corner by means of microscopic observation, thermal analysis and X-ray diffraction analysis [12], and the assessed isothermal section at 335 °C was demonstrated. It is noted that in the work of Liang et al. [2], the experimental investigation of isothermal section at 335 °C was also performed and the comparison between the calculated and experimental results was presented.

In the experimental work by Wang et al. [13], the solidification behavior of Mg–9 wt.% Al–*X* wt.% Zn with $X = 0$, 0.4, 0.8 and 1.2 has been investigated by means of thermal analysis and microstructural observation. Since the cooling rate was fast (30 K/min) in their experiment, the solidification proceeds under non-equilibrium conditions. Based on the cooling curves, they determined a start-solidifying temperature (near liquidus) and end-solidifying temperature.

Among the above-mentioned literatures, all the experimental work except for Refs. [6,13] were taken into account in the work of Liang et al. [2]. Even though, a comprehensive and explicit comparison for the Mg-rich alloys had not been given in that work.

3. Experimental procedure and results

The chemical compositions of Mg-alloys investigated in the present work are shown in Table 1. The compositions for the elements of our concern, i.e., Al and Zn, are denoted in bold letters. These alloys were prepared using following pure materials: Mg bars, min. 99.9 wt.% provided by Norsk Hydro Magnesiumgesellschaft mbH, Bottrop; Al bars, 99.98 wt.% produced by Hydro Aluminium High Purity GmbH, Grevenbroich and Zn rods, 99.98 wt.% obtained from the Harzer Zink GmbH, Goslar, all purities referred to metal basis. The starting material for each alloy was weighed, melted and held for 10 min at 750 °C in stainless steel crucible with protection by mixture of 0.4 vol.% SF_6 and 3 vol.% Ar in air. The sample was homogenized by mechanical stirring and, then, the melt was cast in a cold heavy steel mold. Typical as-cast weight was 2 kg. The compositions of prepared alloys were analyzed in our chemical laboratory using inductively coupled plasma (ICP).

Pieces of about 0.5 g were cut from the inside of the as-cast sample material. They were analyzed by differential thermal analysis (DTA) and two heat-flow twin cylindrical Calvet-type DSC devices. The DTA measurements were performed using a Netzsch DTA 404 S apparatus (NETZSCH GmbH, Selb, Germany). In preliminary experiments, it was realized that because of high oxygen affinity and vapor pressure of the studied Mg-alloys, a special adaptation of DTA equipment using sealed Ta crucible is indispensable to obtain reproducible and reliable data. The detail of the adaptation is found in Ref. [14]. In the DTA measurement, high purity γ-Al_2O_3 powder was used as the reference material. A standard temperature calibration was

Table 1
Chemical composition of the investigated alloys, balance Mg (wt.%)

Alloy sample	**Al**	**Zn**	Mn	Si	Fe	Cu	Ni	Be
Mg–Al6–Zn1	**6.24**	**0.50**	0.0190	0.017	0.0213	0.0019	0.0005	<0.0001
Mg–Al6–Zn2	**5.61**	**1.70**	0.011	0.013	0.0229	0.0012	0.0004	<0.0001
Mg–Al9–Zn1	**9.43**	**1.21**	0.0064	0.032	0.0062	0.0014	0.0075	<0.0001

The compositions for the elements of our concern, i.e., Al and Zn are denoted in bold letters.

Table 2
Evaluated signal temperatures of the three alloy samples by means of the DSC and DTA measurements in °C

	Mg–Al6–Zn1		Mg–Al6–Zn2			Mg–Al9–Zn1	
	Signal A[a]	Signal B[b]	Signal A[a]	Signal B[b]	Signal C[c]	Signal A[a]	Signal B[b]
DSC1[d] [this work]	611	433	613	415	361	596	431
DSC2[e] [this work]			606	411	360	592	426
DTA [this work]			608	415	Not certain	595	435

[a] Start of the (Mg) precipitation.
[b] Start of the γ-phase precipitation.
[c] Start of the ϕ-phase precipitation (weak signal).
[d] Evaluation from multiple samples and scanning rates.
[e] DSC2 is the experimental data measured with different equipment at Ferro's group.

carried out using the melting point of high purity Al, In, Mg, Pb and Sb elements. The DTA scanning program comprised cycles 330–650–330 °C at heating/cooling rates of 1 and 5 K/min. The measurements were carried out at 5×10^{-3} mbar static external vacuum to protect the Ta-capsule outer surface against oxidation and to eliminate convective heat exchange in gas inside the chamber. The overall uncertainty of the DTA measurements was estimated to be ±3 K.

The DSC measurements are performed by using Setaram MHTC 96 DSC equipment. The equipment was calibrated using high purity Ag, Cu, In, Mg and Pb. Helium at 2 l/h flow rate has been applied as analysis chamber gas. The sealed Ta-capsule was also used due to the above-mentioned reasons. The sample Ta-capsules were filled up to 50 vol.% with the sample material and sealed under argon with 0.5 bar over pressure by electric arc welding. The average empty Ta-capsule weight was 2950 ± 30 mg, and the typical sample weight was about 400 mg. The reference Ta-capsule was also sealed by welding, and a sapphire cylinder was used as reference material. The sapphire mass was 492.5 mg, which is a good balance for the heat capacity of the sample. Both, the encapsulated sample and reference materials were placed approximately in the middle of the DSC-transducer cell height, as this is the most sensitive zone. The scanning program comprised cycles 150–700–150 °C at heating/cooling rates of 2 and 5 K/min. For each alloy composition, two independent samples were studied and two or three heating/cooling cycles were performed for each sample. The results are consistent and reproducible. No significant dependence on the heating/cooling rates was observed. The overall uncertainty of DSC measurements was estimated as ±3 K for temperature determination.

In addition, the results of DSC measurements performed at the group of Prof. Ferro at the University of Genova are employed for comparison. These DSC measurements were performed by using a Setaram TG-DSC 111 calorimeter. The same scanning program was applied, except for the scanning rate which was set to 3 K/min in their measurement. The purified Ar flow at 2 l/min through measuring chamber was applied. In the present paper, the experimental data measured at Ferro's group are referred to as DSC2 [this work], while the data of our DSC (Setaram MHTC 96) measurement is indicated as DSC1 [this work].

Table 2 shows the experimental results of the DSC and DTA measurements. Two signals A and B were clearly observed in both the measurements. The temperature for the signal A, which corresponds to the liquidus, was evaluated based on the onset of the signal on cooling curve. On the other hand, the temperature for the signal B was evaluated based on the maximum of another signal on heating curve. This point will be discussed in detail in Section 4.4. In addition to strong signals A and B, a weak signal C was observed at lower temperature in the DSC measurements of Mg–Al6–Zn2 alloy. However, this signal could not be detected by the DTA experiment, which may be due to the lower sensitivity of the equipment. The temperature for the signal C was evaluated based on both the onset temperatures on the cooling and the maximum temperature on heating curves. It is noted that according to the device performance and the experimental conditions, such as cooling/heating rate, the results of DSC1 are considered to be most reliable.

The microstructure of the samples after DTA experiments was examined by scanning electron microscopy with energy dispersive X-ray microanalysis (SEM/EDS). The samples were ground and polished down to 1 μm diamond under alcohol to avoid reaction with water. The samples were etched in the solution of 1 cm^3 HNO_3, 20 cm^3 acetic acid, 60 cm^3 ethylene glycol and 19 cm^3 H_2O for 15 s at room temperature. The result of microstructural observation will be discussed in Section 4.4.

4. Comparison of calculated and experimental data and discussion

4.1. Liquidus surface

The software "Pandat"[1] [15] and the thermodynamic descriptions of Liang et al. [2] were employed for all the calculations in this work. It is emphasized that none of the comparisons and data specific to Mg-rich alloys shown below are given in their work [2].

Fig. 1 demonstrates the calculated polythermal projection of liquidus surface with the alloy compositions of the experimental data in the Mg-rich corner. The dashed lines represent the

[1] Pandat—Phase Diagram Calculation Engine for Multicomponent Systems, CompuTherm LLC, 437 S, Yellowstone Dr., Suite 217, Madison, WI, USA.

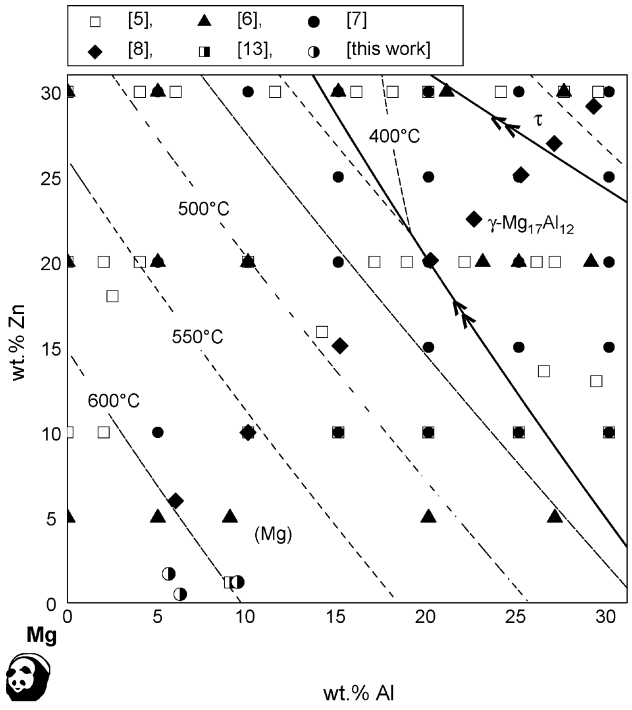

Fig. 1. Calculated partial Mg–Al–Zn liquidus surface and experimental alloy compositions. The thick lines indicate monovariant reaction lines and the dashed lines represent isotherms at an interval of 50 °C.

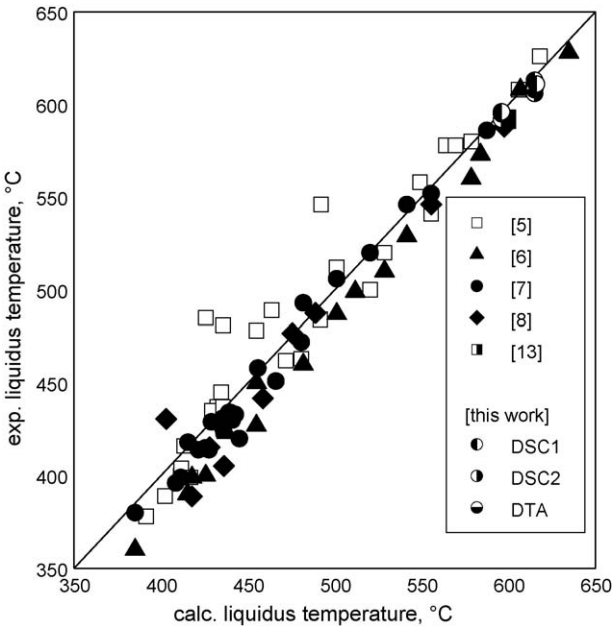

Fig. 2. Comparison between calculated and experimental liquidus temperature for all alloy samples shown in Fig. 1. The straight line is a visual aid corresponding to perfect agreement between experimental and calculated results.

isotherms at an interval of 50 °C and the solid lines indicate the two monovariant reaction lines L + (Mg) + γ-$Mg_{17}Al_{12}$ and L + γ-$Mg_{17}Al_{12}$ + τ. For convenience, the Mg-solid solution is denoted as (Mg) throughout the present paper. As mentioned in Section 2, the experimental results of Refs. [9,10] are not employed in the comparison, because the actual values of the data are not reported in both the literatures. The corresponding detailed comparison between the calculated and experimental liquidus temperatures is shown in Fig. 2. The vertical axis represents the experimental value, while the horizontal axis denotes the calculated value. The liquidus temperatures are calculated at each alloy composition given in Fig. 1. The solid line is a visual aid, indicating the perfect agreement between the experimental and calculated values. One can readily see that the calculated result is in good agreement with the data of Refs. [6–8,13] and this work. Note that the experimental data of this work correspond to signal A given in Table 2. It is seen in Fig. 2 that some of the experimental data of Ref. [5] deviate from the calculated and other experimental results. From a closer look at Fig. 2, furthermore, one can realize that below 450 °C, the calculated values are slightly higher than most of the experimental data. This temperature range corresponds to high alloy compositions and the primary phase fields of γ-$Mg_{17}Al_{12}$ or τ. The supercooling effect in the thermal analysis may be considered as one of the reasons for this slight discrepancy. Except for such a minor discrepancy, the calculated result obtained by thermodynamic description of Liang et al. [2] is in satisfying agreement with the experimental data. The agreement is especially good at the high temperature end, that is, for the most relevant industrial Mg-alloy range including the own key experiments. It should be pointed out that this type of Calphad analysis enables us to identify systematic trends between groups of experimental data.

The comparison of reported primary crystallizing phases to the phase fields is shown in Fig. 3. The calculated liquidus surface is identical to the one shown in Fig. 1, except that the interval of the isotherms is 25 °C in Fig. 3. The calculated result agrees well with the experimental data. As mentioned in Section 2, the primary phase "$MgZn_2$" determined in Ref. [7] has been corrected as the primary τ-phase in the later assessment [3]. Also,

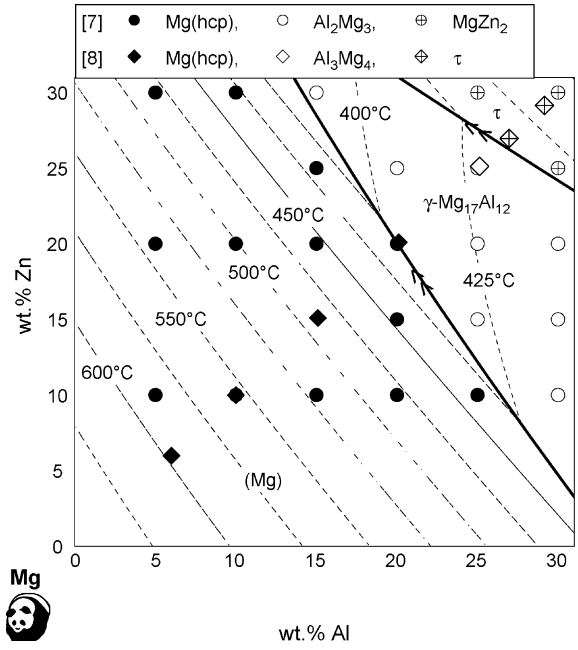

Fig. 3. Calculated liquidus surface and experimental results for the primary precipitates. Compared to Fig. 1 the interval of isotherms is halved to 25 °C.

"Al_2Mg_3" in Ref. [7] and "Al_3Mg_4" in Ref. [8] correspond to γ-$Mg_{17}Al_{12}$ phase in the present calculation. It should be pointed out that the monovariant reaction line of L + (Mg) + γ-$Mg_{17}Al_{12}$ is crucially important to describe solidification process of Mg-alloys with high degree of accuracy. The calculated monovariant line is quite consistent with the experimental data.

4.2. Vertical phase diagram sections

The vertical Mg–Al–Zn phase diagram sections of the Mg-rich corner are demonstrated in Fig. 4 with the experimental data obtained by thermal analysis [5–8]. One can see the satisfying agreement between the calculated results and the experimental

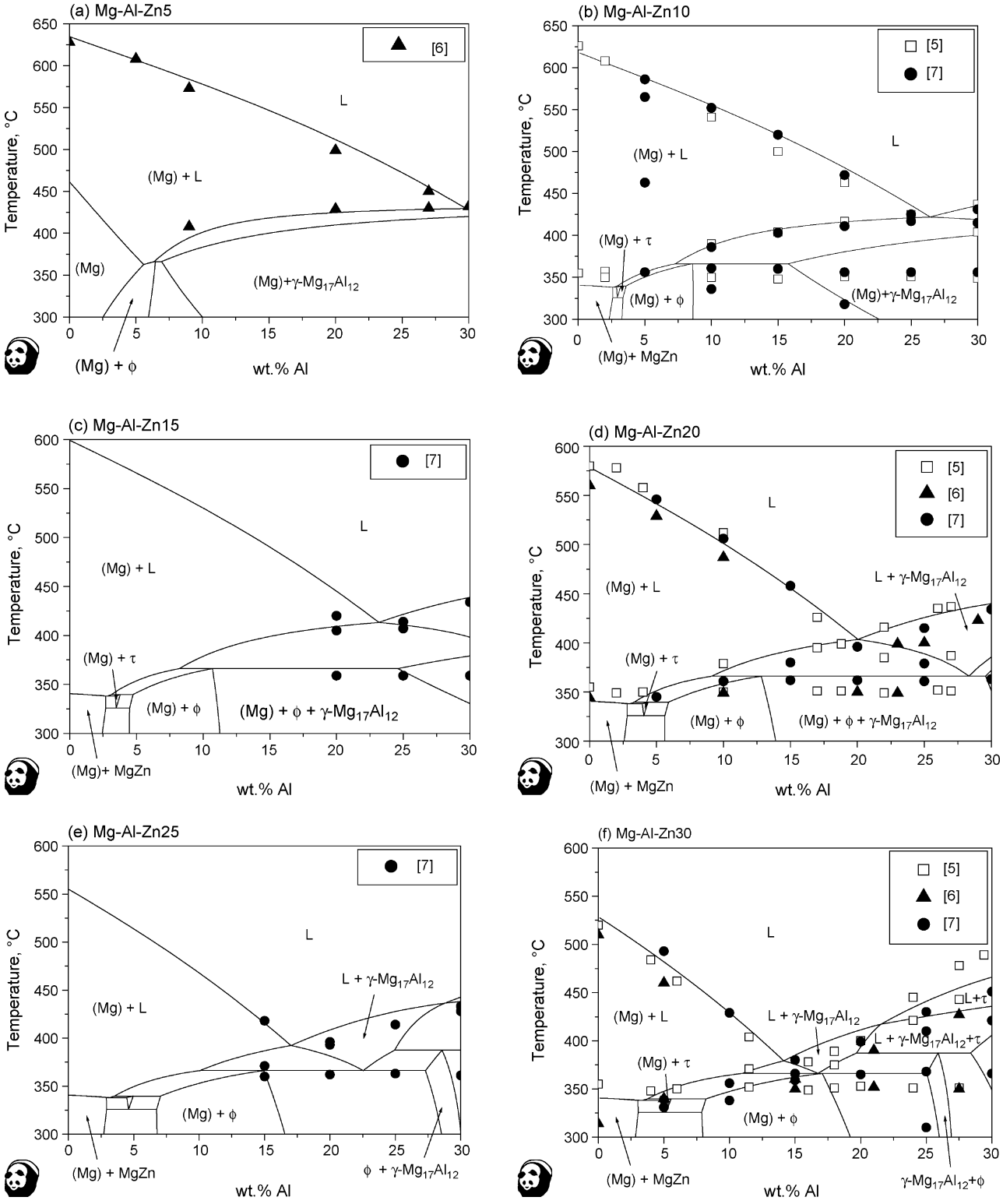

Fig. 4. Calculated vertical sections of the Mg–Al–Zn phase diagram at fixed compositions with the experimental data of thermal analysis: (a) 5 wt.% Zn, (b) 10 wt.% Zn, (c) 15 wt.% Zn, (d) 20 wt.% Zn, (e) 25 wt.% Zn, (f) 30 wt.% Zn and (g) Al:Zn = 1:1 weight ratio.

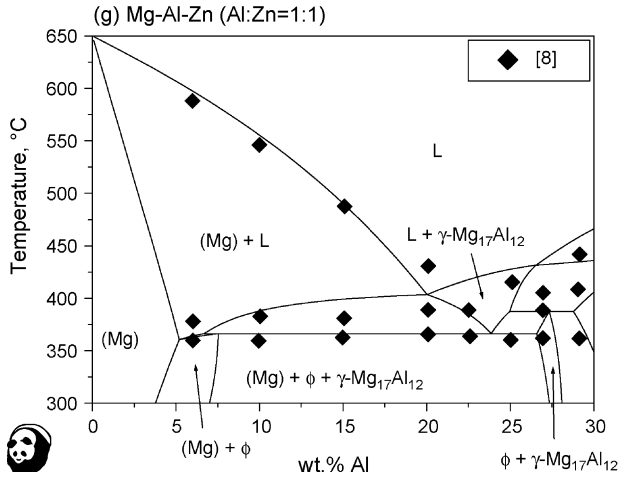

Fig. 4. (*Continued*).

data. Especially the calculated liquidus temperature for primary solidification of Mg-solid solution agrees very well with the experimental one, as summarized in Fig. 2. It should be pointed out here that all the thermal signals at low temperature shown in Fig. 4 are associated with phase equilibria involving more than two solid phases and there is no experimental data of alloy composition where the solidification process ends up in the single-phase field of Mg-solid solution. As demonstrated later (Fig. 8), however, most of the practically important Mg-alloys have the single-phase field of Mg-solid solution just below the solidus temperature and, in such a case, the result of thermal analysis requires a careful interpretation, which is our main concern in Section 4.4.

The experimentally observed number of equilibrium phases at a given temperature [7] is compared in Fig. 5 to the calculated vertical phase diagram sections at constant 10 or 30 wt.% Zn. In that experimental work [7], the samples were heated for 1 or 2 h at a given temperature following pre-heating for 75 h at 300 °C. Then, after quenching, the number of equilibrium phases at a given temperature was determined based on microstructural observation of samples. The overall consistency between the calculated and the experimental results can be seen in both the figures. However, slight discrepancies are observed regarding solid phase equilibria at low temperatures, i.e., below about 350 °C. Based on our experience an equilibration period of a total of up to 77 h at 300 °C may not be sufficient to attain solid state equilibria in Mg-alloys. Also, the microstructural observation necessarily involves difficulty in detecting a small amount of solid phases.

4.3. Solidus and solvus temperatures

As mentioned in Section 2, the solidus isotherms were reported by Mikheeva and Krjukova [11], while the actual values of the experimental data were not given. Since no other experimental work for the solidus isotherms could be found in published literature, the solidus curves are extracted from graphical result of their work [11] and compared with the calculated result. Fig. 6 represents the calculated (solid line) and the exper-

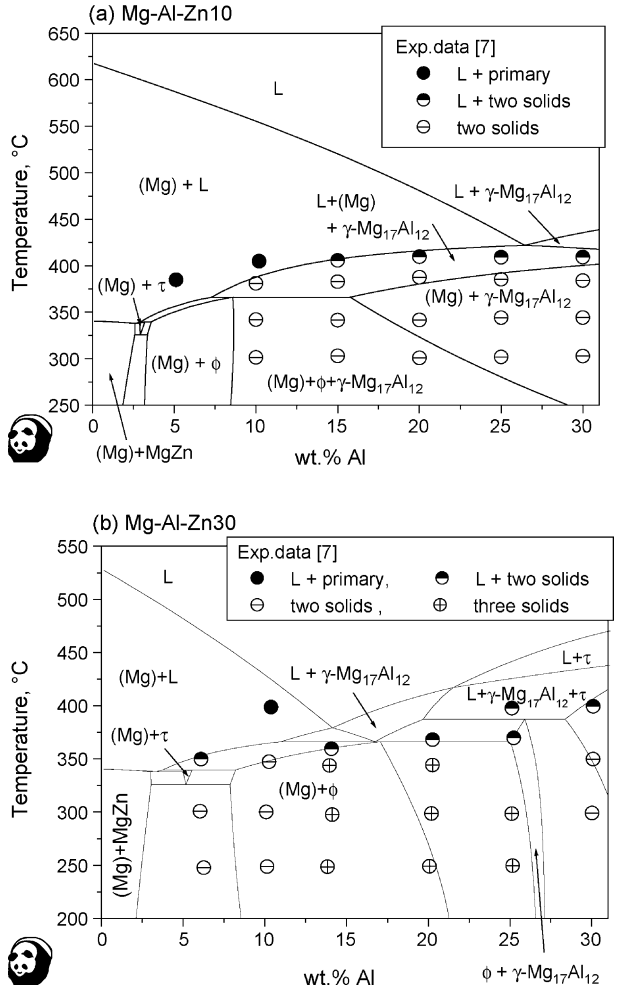

Fig. 5. Calculated vertical sections and the experimental results for the number of equilibrium phases at a given temperature [7]: (a) 10 wt.% Zn and (b) 30 wt.% Zn.

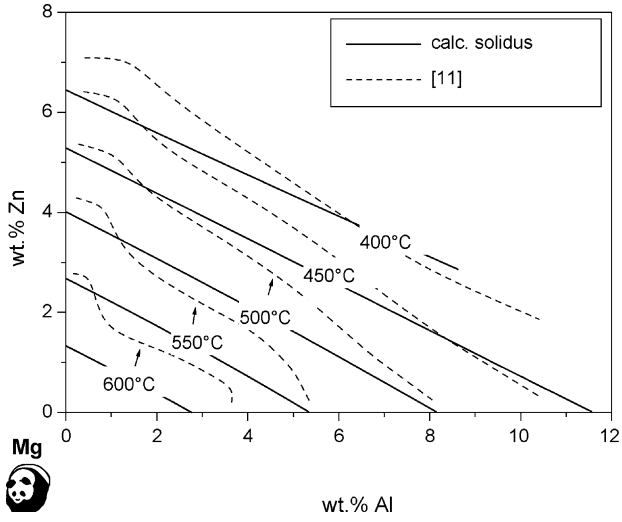

Fig. 6. Solidus isotherms calculated (solid line) and experimentally reported in [11] (dashed line).

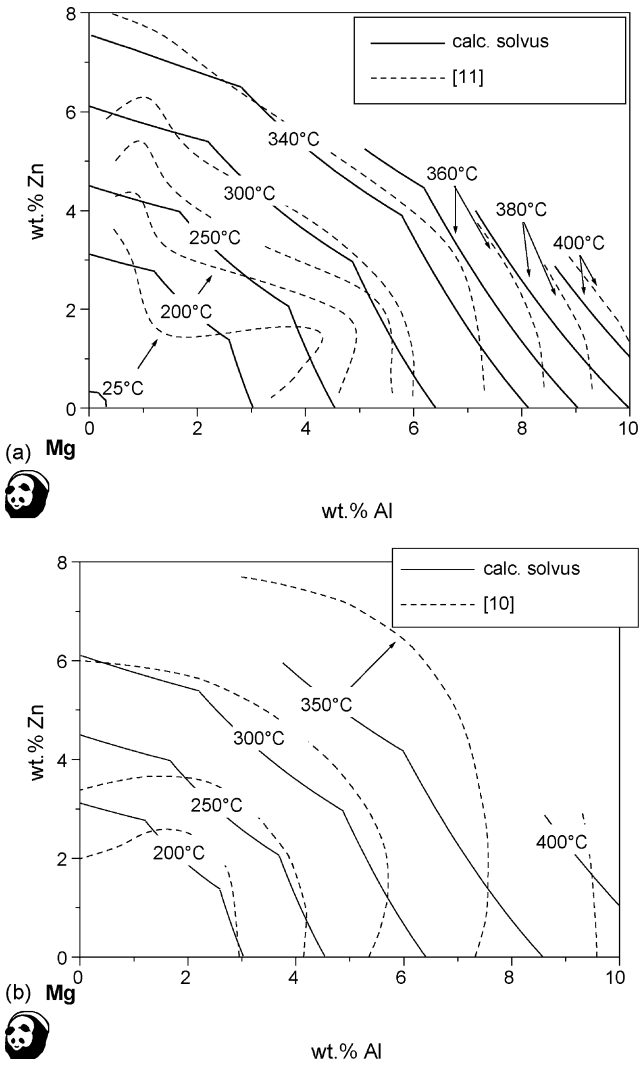

Fig. 7. Solvus isotherms calculated (solid line) and experimental results (dashed line): (a) [11] and (b) [10].

imental solidus isotherms (dashed line). Note that the phase field just below this solidus surface is single-phase field of Mg-solid solution. The calculated result is at least qualitatively consistent with the experimental one. However, Zn-solubility in Mg reported in Ref. [11] mostly takes higher value than the calculated one. This inconsistency is noticeable even in binary Mg–Zn edge. Since the calculated solidus temperature in Mg–Zn binary edge is well supported by the experimental data for the binary system [2], the high value of Zn composition claimed in the ternary work [11] is considered to be unreliable.

The solvus isotherms for Mg-solid solution were demonstrated in Refs. [10,11]. Since, again, the actual values of the experimental data were not shown in both the literatures, the solvus isotherms are extracted from their graphical results and compared in Fig. 7 with the presently calculated result. Note that both these experimental results are not consistent with each other. Because the experimental procedures were not explained in detail in those papers [10,11], the reliability for both the experimental data sets cannot be discussed. It is obvious that the plotted "experimental lines" do not comply with the clear and sharp bends required by thermodynamics at the change of the precipitating phases. For example, following the 300 °C isotherm in Fig. 7(a or b) from Zn-rich to Al-rich alloys, the precipitation of three different phases is encountered, MgZn, ϕ and γ-$Mg_{17}Al_{12}$. Thus, the homogeneity range of Mg-solid solution cannot be bordered by one smooth curve but by three sections of curves as given correctly by the present thermodynamic calculation.

However, the calculated results agree by and large reasonably well with the experimental results, except for the following points where the disagreement between both of the experimental data sets is noticeable. In Fig. 7(a), the ternary solubilities in Mg-solid solution below 250 °C given in Ref. [11] are too large as compared to the calculated results, which is noticeable even in Mg–Zn and Mg–Al binary edges. Since the thermodynamic descriptions for each binary system are well established, the assessed solvus curves of Ref. [11] at low temperature cannot be justified. In Fig. 7(b), the ternary solubility at 350 °C is much larger than the calculated result. This large solubility is also against the experimental work of Ref. [11], when the solubility at 350 °C is interpolated from the ones at 340 and 360 °C in Fig. 7(a). Also the shape of the 350 °C curve is in drastic disagreement with the thermodynamic requirement discussed above. In the original paper [10], the authors have pointed out that additional experiments indicated the solubility at 350 °C which is not as large as shown in their figure, i.e., dashed line in Fig. 7(b). Thus, by and large we can state that the experimental solvus data are fairly consistent with the calculated results.

4.4. Phase equilibria for composition range, 0–10 wt.% Al and 0–3 wt.% Zn

The DSC and DTA measurements of Mg–Al6–Zn1, Mg–Al6–Zn2 and Mg–Al9–Zn1 alloys performed in the present study focus on the composition range of currently important Mg-alloys. The calculated vertical phase diagram sections at a fixed Al composition are shown in Fig. 8. The solid lines present the phase diagrams at nominal Al-content, 6.0 and 9.0 wt.% Al, in Fig. 8(a and b), respectively. The dotted lines are the calculated diagrams for two actual sample compositions of Table 1, 6.24 and 9.43 wt.% Al, respectively. This small variation in Al-content has negligible influence on the liquidus lines and only small influence on solidus and solvus lines. It should be noticed that the Mg-alloys in these dilute Al and Zn composition ranges have single-phase field of Mg-solid solution just below solidus temperature in contrast to the experimentally studied alloys in Fig. 4.

The experimental results of Wang et al. [13] at nominal Al-composition, 9 wt.%, are also indicated in Fig. 8(b). As already demonstrated in Section 4.1, the calculated liquidus temperature is in good agreement with all of the experimental results. However, the calculated solidus temperature appears to disagree with the signal B of this work and "solidus" temperature of Ref. [13]. It should be noted that in the work of Wang et al. [13], the cooling rate was fast (30 K/min) and their data do not represent the equilibrium solidus temperature. In fact, the term "end-solidifying temperature" was used in that work [13]. On the other hand, much lower heating/cooling rate has been used in the present

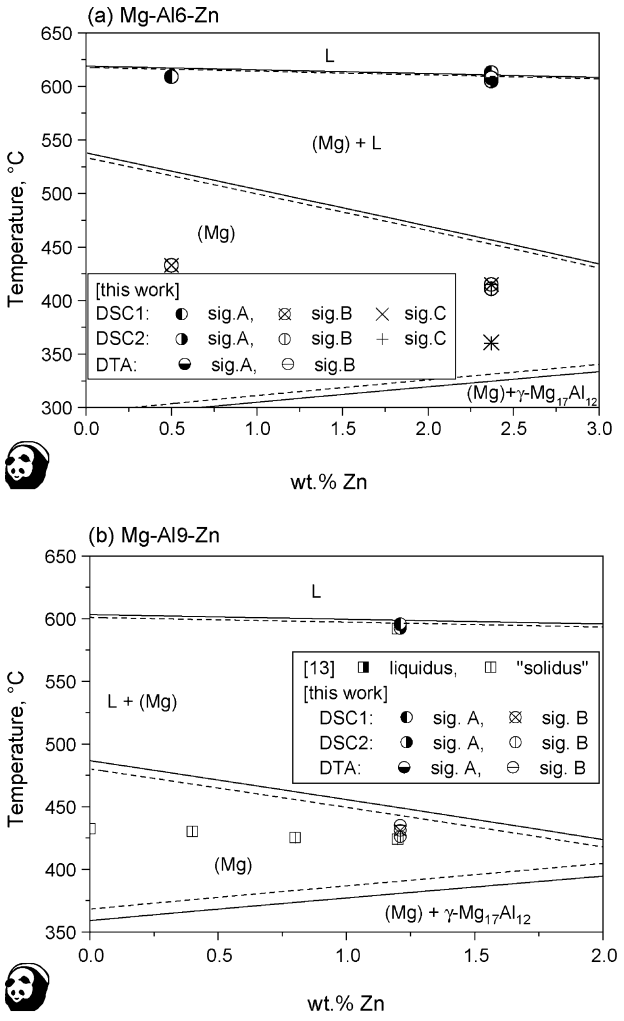

Fig. 8. Calculated vertical sections at fixed Al compositions with the experimental data: (a) Mg–Al6–Zn, solid lines for nominal 6.0 wt.% Al, dotted lines for 6.24 wt.% Al and (b) Mg–Al9–Zn, solid lines for nominal 9.0 wt.% Al, dotted lines for 9.43 wt.% Al.

experiments (1 K/min in DTA, 2 K/min in DSC). As seen in Fig. 8(b), however, the signal B measured in the present study is virtually identical to the experimental data of Ref. [13].

Shown in Fig. 9 is the microstructure of Mg–Al9–Zn1 alloy after the DTA measurement. The dark region corresponds to the matrix of Mg-solid solution. The bright region, which appears along the grain boundary of the matrix, consists of eutectic structure of γ-$Mg_{17}Al_{12}$ and Mg-solid solution having different composition from the matrix. This microstructure suggests that coring of Mg-solid solution takes place during solidification and γ-$Mg_{17}Al_{12}$ phase precipitates directly from the liquid phase. According to the phase diagram (Fig. 8(b)) solidification of this sample should be terminated at a higher solidus temperature without precipitation of γ-$Mg_{17}Al_{12}$ from the liquid. In other words, the solidification proceeds under non-equilibrium condition, even though the cooling rate in our measurement was very low. This can be readily confirmed by performing Scheil calculation as discussed in the following.

Fig. 10(a) shows the DSC curve of Mg–Al9–Zn1 alloy with the scanning rate of 2 K/min. One can clearly see two signals, A and B on both the cooling and heating curves. Fig. 10(b) represents the solidification curve of Mg–Al9–Zn1 alloy calculated under the Scheil conditions. In Fig. 10(b), the solidification starts at 600 °C and the sharp bend in the solidification curve occurs

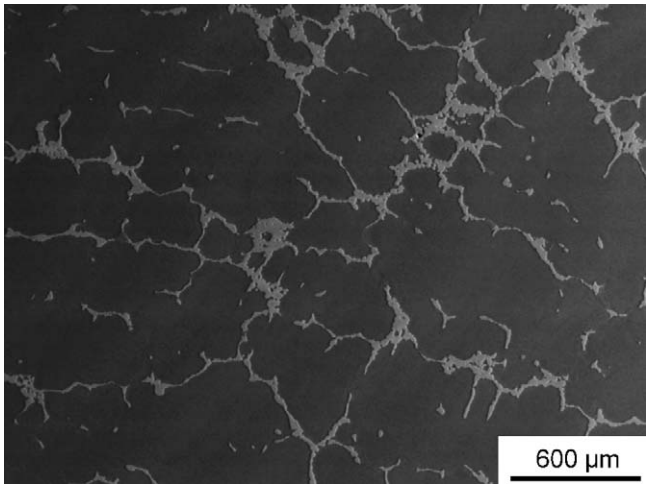

Fig. 9. Microstructure of Mg–Al9–Zn1 sample after the DTA measurement (1 K/min).

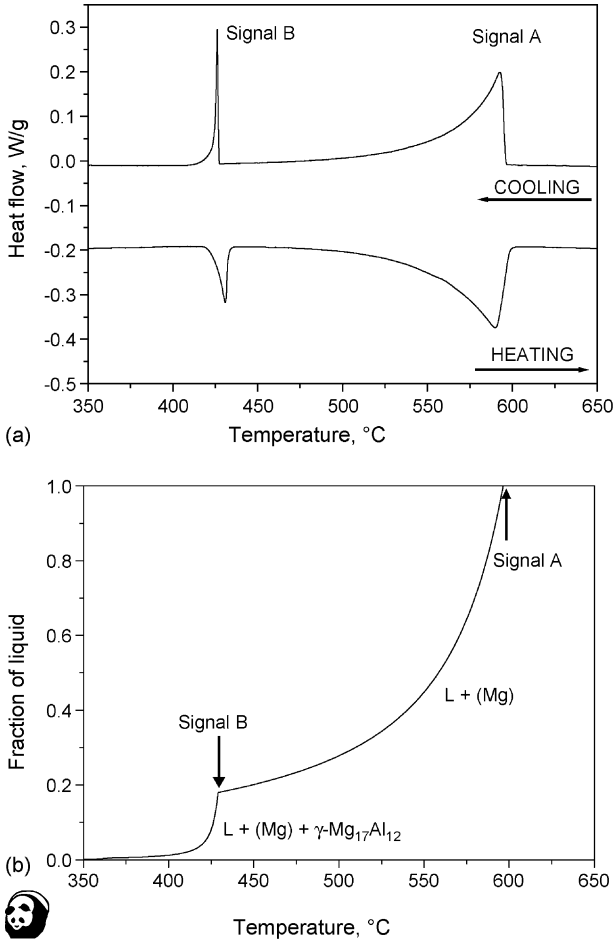

Fig. 10. (a) DSC curve of Mg–Al9–Zn1 alloy measured with heating/cooling rate of 2 K/min and (b) solidification behavior of Mg–Al9–Zn1 alloy calculated by Scheil scheme.

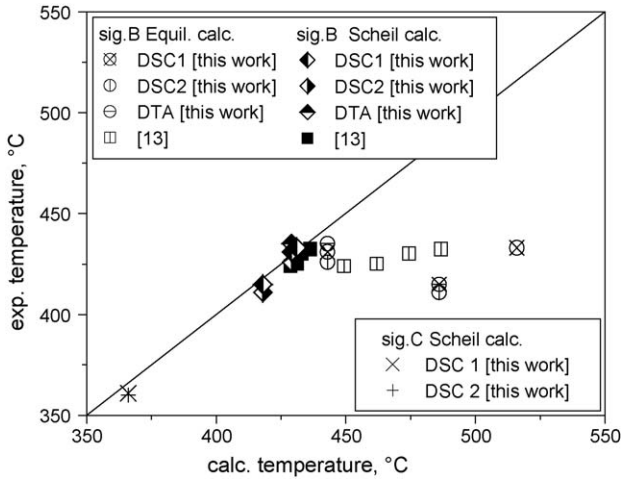

Fig. 11. Comparison of all experimental sub-liquidus thermal analysis data of Fig. 8 to thermodynamic calculations. Open symbols indicate the equilibrium solidus calculations. The calculated results under Scheil conditions for signal B represent the temperature at which monovariant eutectic reaction, $L \rightarrow (Mg) + \gamma\text{-}Mg_{17}Al_{12}$, starts; for signal C it represents the invariant reaction temperature, $L + \gamma\text{-}Mg_{17}Al_{12} \leftrightarrow (Mg) + \phi$. All calculations are based on actual alloy compositions.

at 429 °C, which corresponds to the temperature for the start of the monovariant eutectic reaction, $L \rightarrow (Mg) + \gamma\text{-}Mg_{17}Al_{12}$, under Scheil conditions. Note that the fraction of liquid phase drastically decreases when $\gamma\text{-}Mg_{17}Al_{12}$ phase starts to precipitate, giving rise to a clear thermal signal that could also be seen from a calculated enthalpy curve of that alloy, not shown here. On the other hand, when the solidification proceeds under equilibrium condition, the precipitation of $\gamma\text{-}Mg_{17}Al_{12}$ phase does not occur and the solidification ends up with the primary Mg-solid solution at 443 °C. From the comparison between Fig. 10(a and b), one can realize that the signal B is closely related to $L + (Mg)/L + (Mg) + \gamma\text{-}Mg_{17}Al_{12}$ transition. This is quite consistent with the microstructural observation discussed in Fig. 9. Note that, in Fig. 10(a), there exists slight temperature difference between the onset of signal B on cooling curve and the maximum of signal B on heating curve. This is because the supercooling effect on precipitation of $\gamma\text{-}Mg_{17}Al_{12}$ phase may occur during cooling cycle. As mentioned in Section 2, the temperature for signal B has been assessed based on the maximum of heating curve. This temperature is related to complete melting of eutectic structure of $\gamma\text{-}Mg_{17}Al_{12}$ and (Mg) phases along grain boundary during heating cycle, which is equivalent to the temperature at which the monovariant eutectic reaction starts during cooling cycle without supercooling effect.

Fig. 11 represents the detailed comparison between the calculated results and the experimental data concerning the signal B of the present work and the "solidus" of Ref. [13]. The vertical axis represents the experimental value and the horizontal axis indicates the calculated values. Two types of calculated results are shown in Fig. 11; one is equilibrium solidus temperature (open symbols) and the other is the temperature at which the monovariant eutectic reaction $L + (Mg) + \gamma\text{-}Mg_{17}Al_{12}$ starts under the Scheil condition. The experimental data are in much better agreement with the calculated results of Scheil condition compared to the assumption of equilibrium. Furthermore, the solely primary equilibrium solidification $L \rightarrow (Mg)$ cannot produce the two distinct signals A and B, which are in perfect agreement with the primary and secondary solidification steps predicted by the Scheil calculation and also seen in the microstructure. It should be stressed that the low temperature signal in thermal analysis for Mg-alloys (signal B in this work) does not represent the end of solidification; the solidification process finishes at much lower temperature under Scheil condition as exemplified in Fig. 10(b). By contrast, the equilibrium solidus point of that alloy is 443 °C.

In addition to two signals A and B, as mentioned in Section 3, the signal C was observed in the DSC measurements for Mg–Al6–Zn2 alloy. The DSC curve of Mg–Al6–Zn2 alloy in the vicinity of signal C is represented by solid line in Fig. 12(a). For the sake of comparison, also, the DSC curve of Mg–Al6–Zn1 alloy, in which signal C was not observed, is indicated by dashed line in Fig. 12a. One sees that there exists the small though distinct peak of signal C on both the heating and cooling curves for Mg–Al6–Zn2 alloy. Fig. 12(b) demonstrates the solidification curves of Mg–Al6–Zn2 alloy (solid line) and Mg–Al6–Zn1 (dashed line) calculated by Scheil scheme. In the calculated solidification curve of Mg–Al6–Zn2 alloys (solid line), the pre-

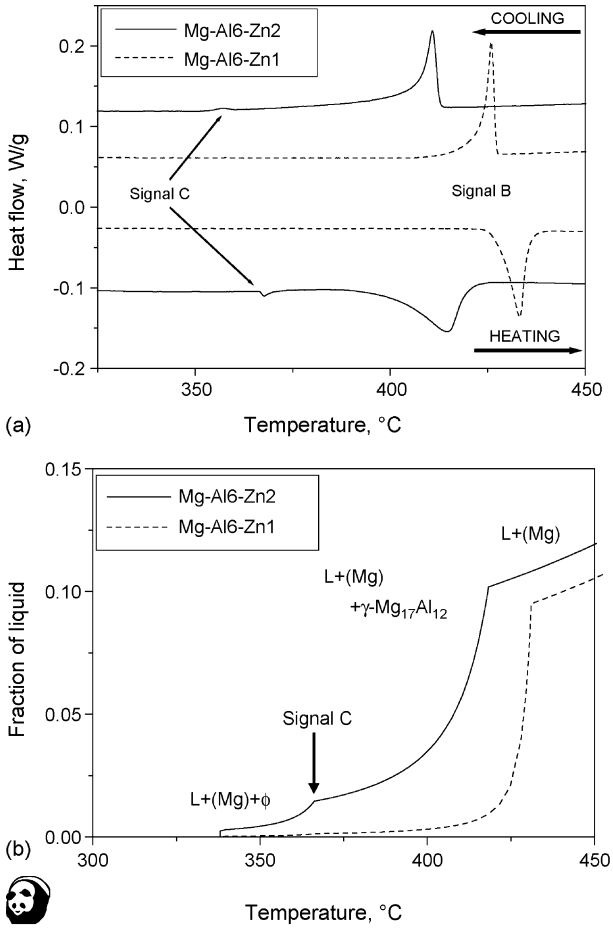

Fig. 12. (a) DSC curves of alloys Mg–Al6–Zn2 (solid lines) and Mg–Al6–Zn1 (dashed lines) in the vicinity of signal C and (b) solidification behavior of alloys Mg–Al6–Zn2 (solid line) and Mg–Al6–Zn1 (dashed line) calculated by Scheil scheme.

cipitation of γ-$Mg_{17}Al_{12}$ phase takes place at 418 °C and, furthermore, the ternary intermetallic compound, ϕ-phase, starts to precipitate at 366 °C. From the comparison between the DSC curve and the sharp bend in the Scheil calculated curve, one can grasp that the signal C is closely related to the precipitation of ϕ-phase. The precipitation of ϕ-phase starts at the invariant reaction temperature, L + γ-$Mg_{17}Al_{12}$ ↔ (Mg) + ϕ, 366 °C. More precisely, since this reaction requires the dissolution of γ-$Mg_{17}Al_{12}$ phase, this four-phase reaction type cannot be realized under Scheil condition and the precipitation of ϕ-phase virtually starts just below this invariant reaction temperature. In Fig. 11, the signal C is compared with the calculated invariant reaction temperature. One can see the good agreement between them. It should be pointed out that in the case of Mg–Al6–Zn1 alloy, also, the precipitation of ϕ-phase occurs during the calculated solidification process (dashed line in Fig. 12(b)). However, this is not visible in the solidification curve because of very small amount of ϕ-precipitate and this is quite consistent with the fact that the signal C was not detected in Mg–Al6–Zn1 alloy (dashed line in Fig. 12(a)). The Scheil calculation also showed that very small amount of ϕ-phase precipitates in the case of Mg–Al9–Zn1 alloy. It should be noted that even the signal C does not represent the end of solidification and solidification process finishes at lower temperature.

It is emphasized that the above discussion concerns only the lower alloyed samples of Fig. 8, where an equilibrium solidification should involve only the L + (Mg) phase field, terminating at the single-phase solid solution and substantially higher temperature. The real solidification inflicts a qualitative and drastic change: all these alloys encounter a three-phase reaction at lower temperature due to the non-equilibrium segregation. By contrast, the higher alloyed samples shown in Fig. 4 encounter the three-phase and higher order reactions even under equilibrium conditions. Therefore, a reasonable agreement of thermal signals with the calculated phase diagrams is observed, even though some shift in the solidification path of these alloys due to segregation is expected and may be calculated. This effect is not as strong as shown in Fig. 11 for the lower alloyed samples.

As discussed above, all the experimental results can be successfully explained by the present thermodynamic calculation, either under equilibrium or under Scheil conditions. This fact strongly supports the reliability of the thermodynamic description of Liang et al. [2] specifically for the Mg-rich alloys.

5. Conclusion

In the present study, focusing on Mg-rich alloys, we have discussed the reliability of thermodynamic description of the Mg–Al–Zn system [2]. The good agreement between the experimental and the calculated results strongly supports the reliability of the thermodynamic description. Also, we investigated solidification and melting of alloys in the practically important composition range by means of DTA and DSC measurements and compared the experimental results with thermodynamic calculations. The following most important results are highlighted:

(i) Even though we have used very slow cooling rate in thermal analysis (1 K/min in DTA, 2 K/min in DSC), the solidification path is far from equilibrium condition and is close to Scheil condition. There is virtually no difference between the results measured with cooling rates of 1 and 30 K/min.
(ii) The low temperature signal B observed in thermal analysis and often claimed as “solidus” is not the equilibrium solidus temperature and is not even the end of non-equilibrium solidification process. This signal corresponds to the start of the monovariant eutectic reaction, L → (Mg) + γ-$Mg_{17}Al_{12}$.
(iii) The lowest signal C observed in the DSC measurement of Mg–Al6–Zn2 alloy represents the precipitation of ϕ-phase. It is consistent that this signal was not observed in the Mg–Al6–Zn1 and Mg–Al9–Zn1 alloys, because the Scheil calculation shows that the precipitation of ϕ-phase occurs in both these alloys in minute amounts only; the solidification process finishes at lower temperature.
(iv) The fact that all the experimental results can be well interpreted by the present thermodynamic calculation strongly supports the reliability of the thermodynamic description of Liang et al. [2]. This thermodynamic description is now well established also in the Mg-rich corner and enables a proper interpretation of experimental results obtained under equilibrium and non-equilibrium conditions.

Acknowledgements

The present authors are grateful to Prof. R. Ferro at the University of Genova for performing the comparative DSC measurements (DSC2). This study is supported by the German Research Foundation (DFG) in the Priority Programme “DFG-SPP 1168: InnoMagTec” under grant no. Schm 588/29.

References

[1] M. Ohno, R. Schmid-Fetzer, Z. Metallkd. 96 (2005) 857.
[2] P. Liang, T. Tarfa, J.A. Robinson, S. Wagner, P. Ochin, M.G. Harmelin, H.J. Seifert, H.L. Lukas, F. Aldinger, Therm. Acta 314 (1998) 87.
[3] D.A. Petrov, Ternary alloys, in: G. Petzow, G. Effenberg (Eds.), A Comprehensive Compendium of Evaluated Constitutional Data and Phase Diagrams, vol. 7, VCH Verlag, Weinheim, Germany, 1993, p. 57.
[4] P. Villars, A. Prince, H. Okamoto, Handbook of Ternary Alloy Phase Diagrams, vol. 4, 1995, p. 3933.
[5] G. Eger, Int. Z. Metallogr. 4 (1913) 50 (in German).
[6] S. Ishida, Nippon Kogyo. Kaishi 49 (1929) 256 (in Japanese).
[7] M. Hamasumi, J. Iron Steel Inst. Jpn. 22 (1936) 258 (in Japanese).
[8] W. Köster, W. Dullenkopf, Z. Metallkd. 28 (1936) 363 (in German).
[9] V.I. Mikheeva, O.N. Krjukova, Dok. Akad. Nauk SSSR 50 (1945) 234 (in Russian).
[10] R.S. Busk, R.F. Marande, Trans. Am. Inst. Miner. Metall. Pet. Eng. 166 (1946) 346.
[11] V.I. Mikheeva, O.N. Krjukova, Dok. Akad. Nauk SSSR 50 (1945) 247 (in Russian).
[12] J.B. Clark, Trans. Am. Soc. Met. 53 (1961) 295.
[13] Y. Wang, Q. Wang, C. Ma, W. Ding, Y. Zhu, Mater. Sci. Eng. A 342 (2003) 178.
[14] D. Mirkovic, R. Schmid-Fetzer, Z. Metallkd., submitted for publication.
[15] S.-L. Chen, S. Daniel, F. Zhang, Y.A. Chang, W.A. Oates, R. Schmid-Fetzer, J. Phase Equilib. 22 (2001) 373.